Low-spin excitations in ^{89}Br populated in β^- decay of ^{89}Se

T. Rząca-Urban,[1,*] K. Sieja,[2] M. Czerwiński,[1] J. Kurpeta,[1] M. Pomorski,[1] W. Urban,[1] J. Wiśniewski,[1] M. Wróblewski,[1] L. Canete,[3] T. Eronen,[3] S. Geldhof,[3] A. Jokinen,[3] A. Kankainen,[3] I. D. Moore,[3] D. Nesterenko,[3] H. Penttilä,[3] I. Pohjalainen,[3] S. Rinta-Antila,[3] A. de Roubin,[4] and M. Vilén[3]

[1]*Faculty of Physics, University of Warsaw, ulica Pasteura 5, PL-02-093 Warsaw, Poland*
[2]*Université de Strasbourg, IPHC, CNRS, UMR7178, 67037 Strasbourg, France*
[3]*University of Jyväskylä, Department of Physics, P.O. Box 35, FI-40014 University of Jyväskylä, Finland*
[4]*Institute for Nuclear and Radiation Physics, KU Leuven, B-3001 Leuwen, Belgium*

(Received 28 April 2022; accepted 1 August 2022; published 18 August 2022)

Low-spin, excited states of the ^{89}Br nucleus, populated in β^- decay of ^{89}Se have been studied for the first time. The ^{89}Se nuclei were produced in proton-induced fission of natural thorium using the IGISOL facility and separated using a dipole magnet and the coupled JYFLTRAP Penning trap. Gamma radiation following the β^- decay of ^{89}Se was measured with an array of high-resolution germanium detectors. Levels scheme of ^{89}Br was extended by 12 new levels and 31 new γ transitions. Spin-parity $(3/2^+)$ has been proposed for the ground state of the ^{89}Se mother nucleus, replacing the $(5/2^+)$ assignment reported in data bases. The observed Gamow-Teller β^- transition to the 1754.5-keV level indicates a $\pi g_{9/2}$-based configuration. The level scheme of ^{89}Br has been compared to large scale shell-model calculations. Excitations based on $\pi p_{3/2}$ and $\pi f_{5/2}$ single-particle levels as well as their anomalous coupling are proposed to explain the low-energy excitation scheme of ^{89}Br.

DOI: 10.1103/PhysRevC.106.024322

I. INTRODUCTION

Neutron-rich nuclei from the region of mass number $A \approx 90$ are a useful source of information on single-particle (s.p.) and collective excitations competing with each other outside the ^{78}Ni core. With such data contemporary, large-scale shell-model (LSSM) calculations can provide a valuable insight into the fundamental quantum processes behind the shape change and coexistence effects in the $A \approx 100$ nuclei, observed at $Z \approx 40$ and $N \approx 60$ [1]. As discussed in a recent study of Sr ($Z = 38$) isotopes [2,3], the explanation of these spectacular effects is still an open question. However, the remarkable LSSM reproduction of 2^+ excitations in the studied Sr isotopes [2] tells us that these excitations, essential for understanding the evolution of collectivity in the region, are more of a single-particle nature than previously supposed. Furthermore, some puzzling LSSM results on the 0_2^+ levels in these isotopes indicate that we still do not understand the nature of the 0^+ excitations associated with the shape change and coexistence phenomena in nuclei (see Ref. [3] for further discussion). This again emphasizes the need for reliable s.p. input data which, in addition to supporting a better description of nuclei in the region, may bring us closer to answering the thought-provoking question of whether the spherical shell model, as we know it at present, is capable of properly reproducing collective effects emerging in transitional nuclei (see, e.g., the review [4] for further reading).

As discussed in Refs. [2,3], one of the s.p. excitations crucial for the description of the shape effects in the region is the $1g_{9/2}$ proton level. Its excitation energy and population govern the rapid evolution of nuclear deformation and collectivity along isotonic lines between Kr and Ru. The place to test its energy relative to other proton levels in the region, $1f_{5/2}$, $2p_{3/2}$, and $2p_{1/2}$, is near the $Z = 28$ closed shell, where the nuclei exhibit simple excitation patterns, not strongly disturbed by collective effects. However, the experimental accessibility of such nuclei drops quickly when approaching the $Z = 28$ closure. The compromise choice is the Br ($Z = 35$) isotopic chain, where one can access several isotopes above the $N = 50$ closed shell using the available nuclear-spectroscopy techniques in order to obtain an extended, systematic data set for testing the shell model.

The present work reports on the first study of excited levels in ^{89}Br populated in β^- decay of ^{89}Se, complementing a series of recent investigations of Br isotopes [5–10]. It is also worth mentioning the search for the $g_{9/2}$-proton-based excitation in ^{83}As in Ref. [11], which reports a tentative $(9/2^+)$ spin-parity for the level at 2779 keV, used for adjusting parameters of the shell model for the region and applied successfully to reproduce levels in Br [5–10] and Rb [12–14] isotopes. Quite large variations of the $\pi f_{5/2} \rightarrow \pi g_{9/2}$ s.p. energies adopted in various shell-model calculations over the years have been revealed (see, e.g., Ref. [11]). In the present work, we further test the adopted shell-model parameters of Ni78-II effective interactions [5,15] by comparing the LSSM calculations to the experimental information newly obtained for ^{89}Br as well as to the known literature data on its $N = 54$ isotones.

After the Introduction, Sec. II describes the experimental techniques used in the present work. In Sec. III we show details of the data analysis and the results obtained for ^{89}Br.

*Corresponding author: teresa.rzaca@fuw.edu.pl

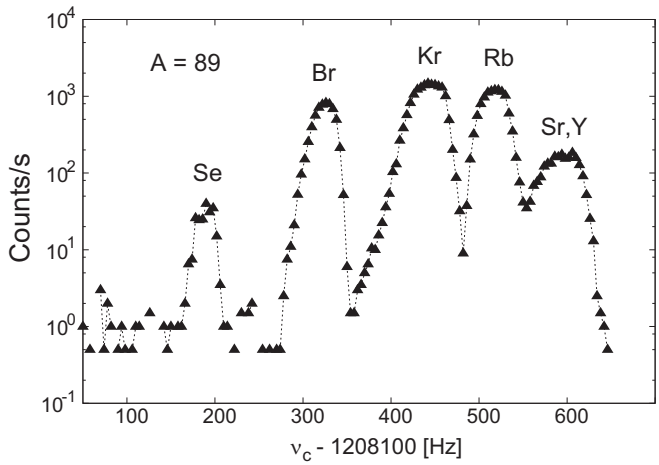

FIG. 1. Ion counts as a function of quadrupole excitation frequency in the purification trap of the JYFLTRAP Penning trap. The mass-separated, singly charged ions of mass $A = 89$ are marked with their element symbols.

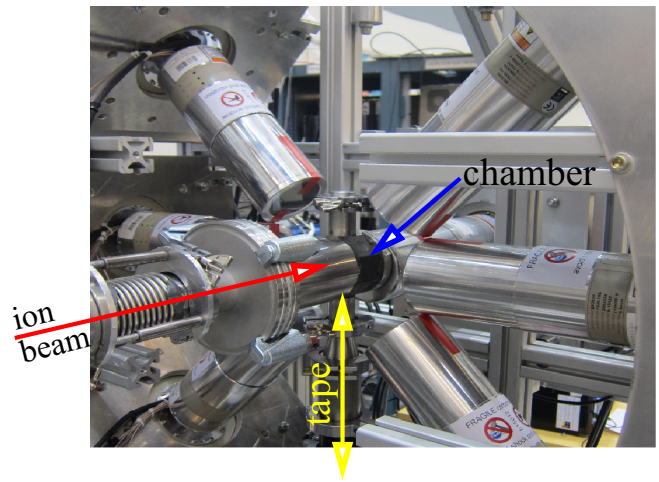

FIG. 2. The γ-detection setup, located after the Penning trap, as used in the present work.

This is followed by the discussion of the results aided by the LSSM calculations which is presented in Sec. IV. Section V summarizes the paper.

II. EXPERIMENTAL TECHNIQUES

The neutron-rich ^{89}Se nuclei were produced in a proton-induced fission reaction [16]. A thin target foil of natural thorium was bombarded with a 30 MeV proton beam from the K-130 cyclotron of the University of Jyväskylä. Fission products were extracted from the gas cell with the sextupole ion guide (SPIG) [17] and accelerated to 30 keV. The fission fragments were then mass separated based on their mass-to-charge ratio m/q using a dipole magnet. The ions were cooled and bunched using a radiofrequency cooler and buncher [18], and further sent to the JYFLTRAP double Penning trap [19]. The ^{89}Se$^+$ ions were selected in the first trap of the JYFLTRAP using the mass-selective buffer gas cooling technique [20]. Figure 1 shows the spectrum of ions with mass $A = 89$, as a function of quadrupole excitation frequency in the first trap, recorded using a microchannel plate (MCP) detector after the Penning trap. The yield of the mass-separated ^{89}Se was about 60 ions/s at the MCP detector. Ions were extracted from the trap every 101 ms and implanted into a movable tape at the center of the detector setup. The tape was moved every 9 s to remove contribution from unwanted long-lived decay products.

An array of seven germanium detectors, shown in Fig. 2, was used to measure γ radiation following β^- decay of ^{89}Se. The array included six high-resolution, broad energy (BE-Ge) detectors mounted in a plane perpendicular to the ion beam direction and one large germanium detector with a relative efficiency of 70%. The BE-Ge detectors, having energy resolutions of 0.4 and 2.0 keV at 5.9 and 1332.5 keV, respectively, were used to measure in detail low-energy γ rays, whereas the large germanium detector was used to register high-energy γ rays. This detector was mounted along the beam axis behind the vacuum chamber containing the tape-transport system (see also Fig. 2 of Ref. [8]). The chamber had Mylar windows allowing the BE-Ge detectors to measure down to 15 keV with high efficiency.

The energy calibration of the detectors was performed using standard calibration sources including ^{133}Ba, ^{60}Co, and ^{152}Eu. In order to fit the γ spectra measured in a 5 MeV energy range into the analyzed 4K-channel histograms without compromising the high resolution of the Be-Ge detectors, we applied so-called constant-peak-width energy calibration, which is a strongly nonlinear calibration, $E_\gamma = C_0 + C_1 \times (\text{channel}) + C_2 \times (\text{channel})^2$, with $C_0 = 0.0$ keV, $C_1 = 0.30$ keV/channel, and $C_2 = 0.000\,284\,404$ keV/channel^2. Such a calibration allows a nonlinear compression of the spectra where the peak width is approximately constant over the whole energy range analyzed. In addition to preserving the high resolution at low energies, it enhances the visibility of high-energy γ lines without losing the resolving power. The high efficiency of the detector setup allowed the collection of about 3.2×10^8 triggerless events in a four-day measurement. The data were collected using the digital gamma finder (DGF) cards with a 40 MHz clock. After the energy recalibration, singles and coincidence γ events were sorted into one-, two-, and three-dimensional histograms for further analysis.

III. ANALYSIS AND RESULTS

A. Data analysis

Despite the excellent separation providing the monoisotopic, β-decaying sample of ^{89}Se at the target position, the analysis of γ decays of excited levels in ^{89}Br measured with the Ge array was not a straightforward task because of the laboratory background radiation, dominating the weak-intensity radiation following β^- decays of the $A = 89$ chain.

Figure 3(a) shows the singles-γ spectrum measured by all seven Ge detectors of the array, where strong background lines are seen. The spectrum is dominated by γ lines of primordial nuclides from the environment such as ^{40}K, ^{238}U, and ^{232}Th

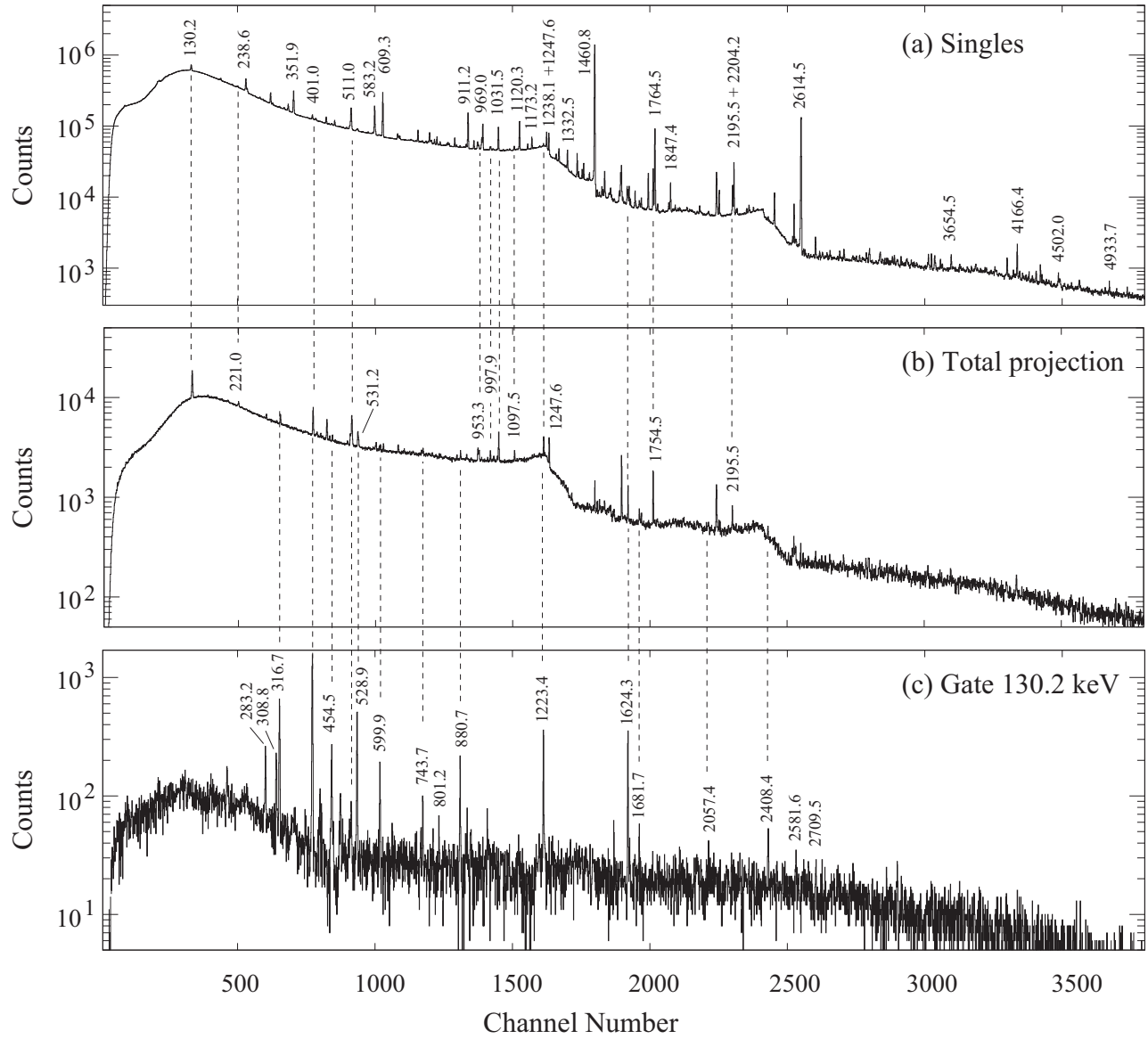

FIG. 3. γ-ray spectra as measured in the present work: (a) singles γ-ray spectrum, (b) total projection of a γ-γ histogram, (c) coincidence γ-ray spectrum gated on the 130.2-keV line. γ lines in the spectra are labeled with energies in keV. The same nonlinear, constant-peak-width energy calibration was applied in all three spectra (see text for details). The description of marked lines with $E_\gamma < 3$ MeV is given in Table I. In panel (a) a few unidentified, high-energy lines are marked.

with their daughters [21], and surrounding background such as ^{60}Co. Also seen are the strongest γ transitions from nuclei populated in β^- decay of the $A = 89$ chain nuclei, though the strongest and the third strongest γ lines of ^{89}Br at 130.2 and 401.0 keV [10] are barely visible in this spectrum. The information on the strongest disturbing γ transitions and the strongest decays in the $A = 89$ chain, marked in the singles spectrum, is summarized in Table I.

Figure 3(b) shows the total projection of the $\gamma\gamma$ histogram measured by all seven Ge detectors of the array. The total number of counts in this spectrum is nearly two orders of magnitude lower than in the singles spectrum. This is due to the 500 ns $\gamma\gamma$ time-coincidence window, which eliminated strong singles lines seen in Fig. 3(a). However, a lot of Compton-scattered events are still present, forming pronounced Compton ridges corresponding to the 1460.8- and 2614.5-keV lines dominating in Fig. 3(a). These are the background coincidence events created in a closely packed Ge array, where strong γ rays backscattered in one of the detectors are recorded in another detector. The 130.2-keV peak dominates the spectrum, and other lines of ^{89}Br are also clearly visible.

Applying gating conditions on the $\gamma\gamma$ histogram allowed further reduction of the contaminating background. In Fig. 3(c) we show a spectrum gated on the 130.2-keV line, reported as the strongest transition in ^{89}Br [10]. The number of counts in the spectrum is reduced by another two orders of magnitude and the 401.0-keV line dominates the spectrum. The new 1754.5-keV line of ^{89}Br, clearly seen in Fig. 3(b), is absent in Fig. 3(c), which suggests that it is in a cascade

TABLE I. Information on the strongest γ-ray transitions observed in the singles spectrum in Fig. 3(a).

Energy (keV)	Nucleus	Source of radiation
130.2	^{89}Br	β^- decay, $A = 89$ chain
221.0	^{89}Rb	β^- decay, $A = 89$ chain
238.6	^{212}Pb	^{232}Th series
351.9	^{214}Pb	^{238}U series
401.0	^{89}Br	β^- decay, $A = 89$ chain
511.0		e^+e^- annihilation peak
583.2	^{208}Tl	^{232}Th series
609.3	^{214}Bi	^{238}U series
911.2	^{238}Ac	^{232}Th series
953.3	^{89}Kr	β^- decay, $A = 89$ chain
969.0	^{228}Ac	^{232}Th series
997.9	^{89}Kr	β^- decay, $A = 89$ chain
1031.5	^{89}Sr	β^- decay, $A = 89$ chain
1097.5	^{89}Kr	β^- decay, $A = 89$ chain
1120.3	^{214}Bi	^{238}U series
1173.2	^{60}Co	surrounding background
1223.4	^{89}Br	β^- decay, $A = 89$ chain
1238.1	^{214}Bi	^{238}U series
1247.6	^{89}Sr	β^- decay, $A = 89$ chain
1332.5	^{60}Co	surrounding background
1460.8	^{40}K	primordial
1624.3	^{89}Br	β^- decay, $A = 89$ chain
1754.5	^{89}Br	β^- decay, $A = 89$ chain
1764.5	^{214}Bi	^{238}U series
1847.4	^{214}Bi	^{238}U series
2195.5	^{89}Sr	β^- decay, $A = 89$ chain
2204.2	^{214}Bi	^{238}U series
2614.5	^{208}Tl	^{232}Th series

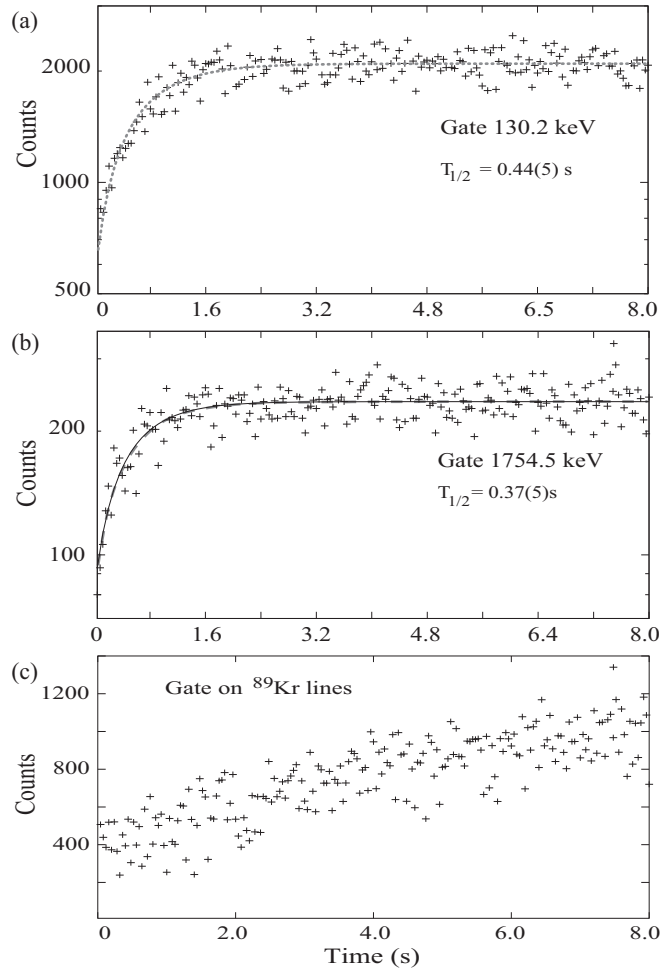

FIG. 4. Time spectra gated on the (a) 130.2-keV γ line of ^{89}Br, (b) 1754.5-keV γ line of ^{89}Br, and (c) γ lines of ^{89}Kr. See the text for more comments.

parallel to the 130.2-keV, ground-state transition. In the following section the 130.2-keV gate and the 1754.5-keV line are discussed in more detail.

B. Properties of the ^{89}Br nucleus

1. Identification of γ lines in ^{89}Br

The 130.2-keV line, reported in Ref. [10] as due to the ground-state transition in ^{89}Br, was first tentatively assigned to ^{89}Br by Rengan *et al.* [22] who suggested that this transition may deexcite a level at 130.2 keV in ^{89}Br because no other γ more intense than the 130.2 keV transition was observed in the β^- decay of ^{89}Br within a time interval of 2 s, and the shape of the ^{89}Br β^- spectrum did not indicate any isomer in ^{89}Br with $T_{1/2} > 2$ s.

In Ref. [10], the 130.2-keV line was observed in prompt, crossover coincidences, with γ lines from the ^{144}La and ^{145}La fission fragments expected to be the most pronounced complementary fragments to ^{89}Br, corresponding to the $3n$ and $2n$ neutron-evaporation channels, respectively. The coincidence with two La isotopes strongly suggested the assignment of the 130.2-keV line to a bromine isotope. Because the 130.2-keV line was not observed in the well-studied ^{87}Br [8,9] and ^{88}Br [5,7] nuclei, it was assigned to a heavier bromine isotope. The ^{89}Br isotope was proposed because the excitation scheme built on top of the 130.2-keV level resembles the excitation scheme of the odd-A ^{87}Br [9] and differs from that of the odd-odd ^{88}Br [5]. The usual identification method using the so-called mass-correlation technique (for a recent example in the region see, e.g., Fig. 3 in Ref. [23]) was not applicable because of rather low intensities of cross coincidences.

In the present work we could uniquely assign the 130.2-keV line to ^{89}Br. First, it is present in the in-beam spectrum, with the $A = 89$ monoisotopic beam on the target, and is absent in the off-beam spectrum measured after the in-beam run. This indicates that it is produced in the β^- decay of the $A = 89$ chain. Second, the time spectrum gated on the 130.2-keV γ line, displayed in Fig. 4(a), shows that its intensity growth corresponds to a $T_{1/2} = 0.44(5)$ s decay half-life, which matches well with the $T_{1/2} = 0.43(5)$ s half-life adopted for the ground state of ^{89}Se [24].

Figure 4(b) shows the time spectrum gated on the newly observed 1754.5-keV γ line. Using such information one can uniquely assign lines to the decay of ^{89}Se, because their intensity-growth pattern differs significantly from the pattern following the decay of ^{89}Br. Figure 4(c) shows the time spectrum corresponding to the summed intensity growth of several

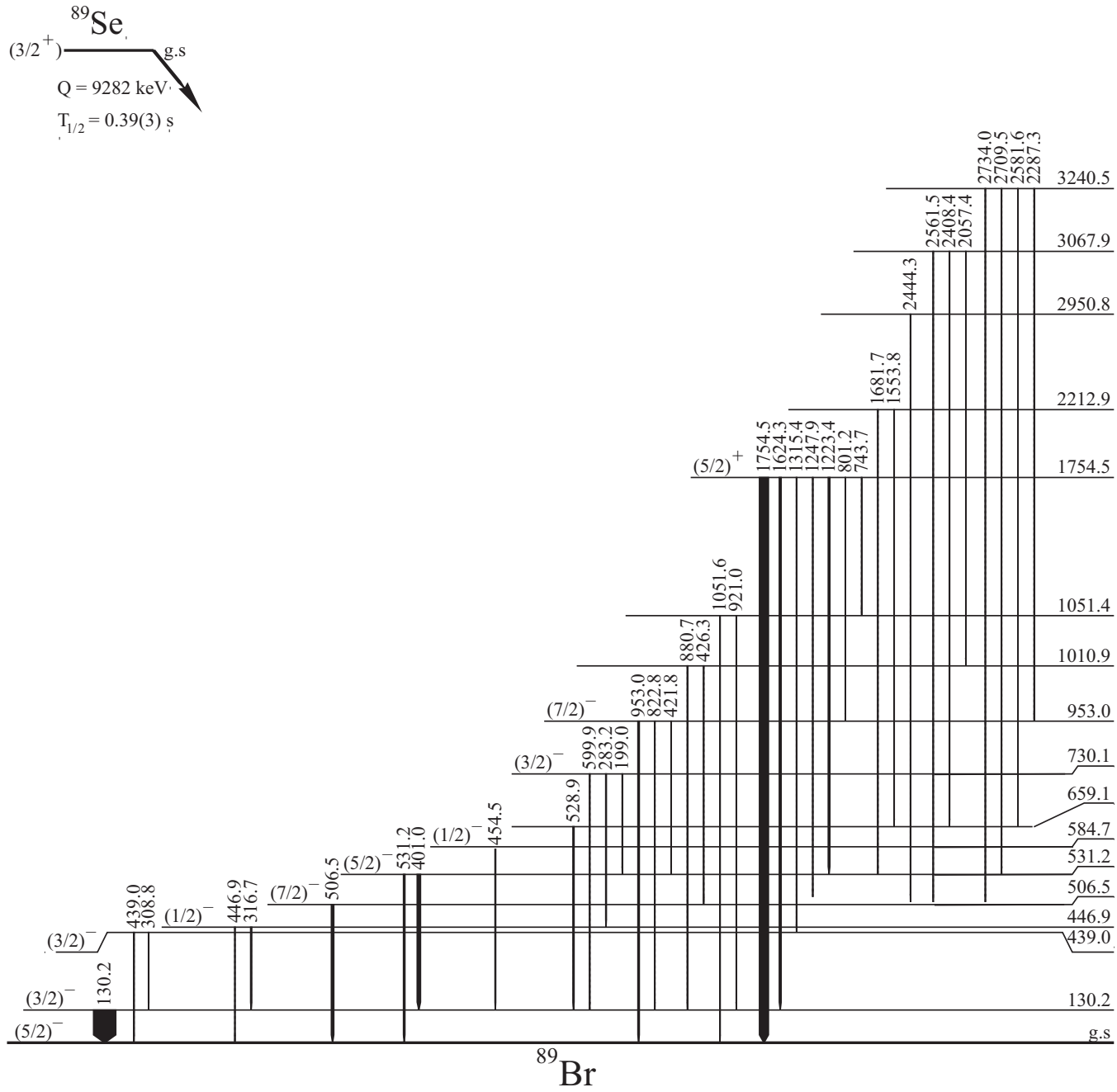

FIG. 5. The scheme of excited levels in ^{89}Br populated in the β^- decay of ^{89}Se, as observed in the present work. The Q_β value was taken from [24]. See text for further information on spin-parity assignments.

γ lines in ^{89}Kr populated in the β^- decay of the ^{89}Br ground state, having the half-life of 3.15(4) min.

The total number of counts in Fig. 4(c) is significantly lower than in Fig. 4(a). This is because most of the β^- activity of ^{89}Br was removed from the target position by the tape. However, not all the activity was taken away because some ions from the trap were scattered elsewhere rather than being deposited on the tape. This caused the nonzero count at channel zero seen in Fig. 4.

The spectra shown in Fig. 4 were measured from the start of the data collection during a 9.00 s tape cycle. To take away the deposited activity the tape was moved during the 0.60 s in the end of each 9.00 s cycle.

2. *The excitation scheme of* ^{89}Br

The construction of the ^{89}Br level scheme shown in Fig. 5 started with the analysis of the γ spectrum gated on the 130.2-keV line. Two fragments of this spectrum are shown in Fig. 6, where one sees the 401.0-, 421.8-, and 822.8-keV lines reported in the prompt-γ measurement [9] and 27 lines corresponding to new transitions in ^{89}Br, placed in the level scheme

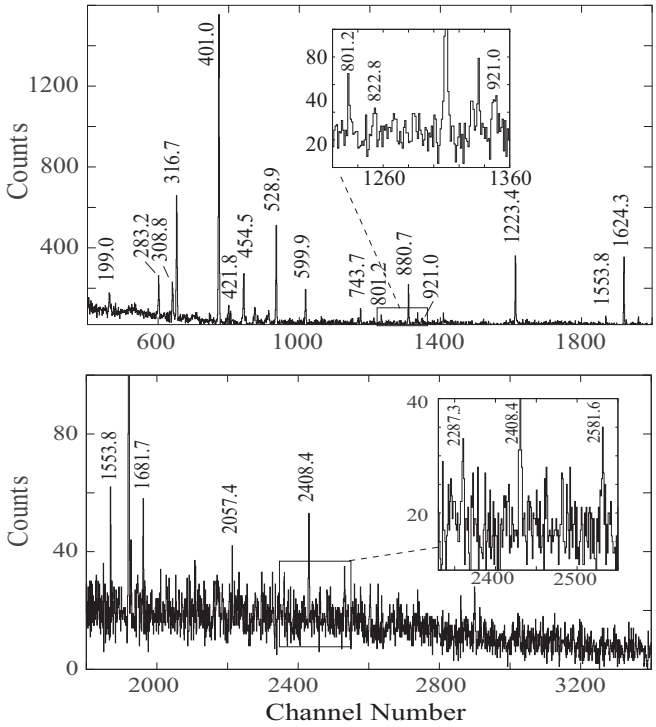

FIG. 6. Two fragments of a γ spectrum gated on the 130.2-keV line of ^{89}Br. Lines are labeled with their γ energies in keV. A nonlinear, constant-peak-width energy calibration was applied, the same as in Fig. 3. See the text for more details.

and listed in Table II. In the 130.2-keV gated spectrum, as well as in the 130.2- 401.0-keV double-gated spectrum, we could not see any trace of the 592.6-keV line corresponding to the transition decaying from the 1545.9-keV, $(9/2^+)$ level reported in Ref. [10].

We also gated on lines corresponding to other ground-state transitions in ^{89}Br, reported in the prompt-γ work [10]. The 506.5-keV gate revealed four new transitions feeding the 506.5-keV level; however, it does not show any trace of the 1039.2-keV transition from the $(9/2^+)$, reported in Ref. [10]. The 531.2-keV gate confirmed the 199.0-, 421.8-, 1223.4-, and 2709.5-keV new lines seen in the 130.2-keV gate.

To search for new ground-state transitions we sorted a specific two-dimensional $\gamma\gamma$ histogram, called γ-S2, where along the γ axis we sorted the two individual energies of a 500-ns $\gamma\gamma$ coincidence event whereas on the S2 axis the sum of these two energies was sorted. This sensitive analysis technique was described in more detail in previous papers (see, e.g., Figs. 3 and 4 and the associated text in Ref. [25]).

Figure 7(a) shows the total projection of the γ-S2 histogram on the S2 axis. The spectrum is dominated by the strong line at 1460.8 keV corresponding to backscattering between detectors of the 1460.8-keV γ rays, seen in Fig. 3(a). There are also peaks corresponding to energy sums of pairs of coincident γ transitions in $A = 89$ nuclei which, except for peaks corresponding to the 531.2- and 1754.5-keV levels in ^{89}Br, are hard to spot. Nevertheless, gating on these lines is very effective. Figure 7(b) shows a spectrum gated on the γ axis on the 130.2-keV line and projected on the S2 axis where these peaks are well seen [note the same abscissa range in Figs. 7(a) and 7(b)].

TABLE II. Properties of excited levels in ^{89}Br including their energies $E_{\rm exc}$, spin-parities I^π, β^- feeding with the corresponding $\log_{10} ft$ values, and the energies E_γ of the depopulating transitions with their relative intensities I_γ, as observed following β^- decay of ^{89}Se measured in the present work.

$E_{\rm exc}$ (keV)	I^π	β feeding (%)	$\log_{10} ft$	E_γ (keV)	I_γ (rel.)
0.0	$(5/2)^-$	20[a]			
130.2(1)	$(3/2)^-$	26(4)	5.5(2)	130.2(1)	1000(42)
439.0(2)	$(3/2)^-$	1.1(3)	6.8(1)	308.8(1)	16(3)
				439.0(1)	24(4)
446.9(2)	$(1/2)^-$	1.6(5)	6.6(2)	316.7(1)	50(5)
				446.9(1)	20(3)
506.5(1)	$(7/2)^-$	3.4(6)	6.3(2)	506.5(1)	110(9)
			8.5(2) 1u		
531.2(2)	$(5/2)^-$	3.9(7)	6.2(1)	401.0(1)	150(9)
				531.2(1)	65(5)
584.7(2)	$(1/2)^-$	1.0(2)	6.8(2)	454.5(1)	31(3)
659.1(2)		0.7(3)	6.9(2)	528.9(1)	51(4)
730.1(2)	$(3/2)^-$	2.8(4)	6.3(1)	199.0(2)	16(3)
				283.2(1)	31(5)
				599.9(1)	20(3)
953.0(2)	$(7/2)^-$	2.8(3)	6.2(1)	421.8(1)	12(3)
			8.5(1) 1u	822.8(2)	3(1)
				953.0(1)	65(5)
1010.9(3)		0.8(2)	6.8(2)	426.3(2)	7(2)
				880.7(1)	23(3)
1051.4(3)		1.1(2)	6.6(2)	921.0(2)	6(2)
				1051.6(2)	20(4)
1754.5(1)	$(5/2)^+$	25(2)	5.1(1)	743.7(2)	9(3)
				801.2(2)	5(2)
				1223.4(2)	75(7)
				1247.9(3)	3(1)
				1315.4(2)	13(3)
				1624.3(1)	84(7)
				1754.5(1)	405(25)
2212.9(3)		0.8(2)	6.5(2)	1553.8(2)	9(3)
				1681.7(2)	11(3)
2950.8(4)		0.5(2)	6.4(3)	2444.3(3)	11(3)
3067.9(3)		1.2(2)	6.0(2)	2408.4(2)	16(3)
				2561.5(3)	10(3)
				2057.4(2)	3(1)
3240.5(3)		1.4(3)	5.9(1)	2287.3(2)	7(2)
				2581.6(3)	9(3)
				2709.5(3)	8(3)
				2734.0(2)	9(3)

[a]Assumed.

A spectrum gated on the 1460.8-keV peak on the S2 axis, displayed in Fig. 8(a), shows a smooth distribution of Compton-scattered energies, with two maxima corresponding to the backscattering of the 1460.8-keV singles line and two weak discrete lines corresponding to the first escape effect.

In contrast, in Fig. 8(b) we show a spectrum gated on the S2 axis on the 1010.9-keV peak (seen in the inset in Fig. 7), corresponding to the 1010.9-keV level in ^{89}Br where one

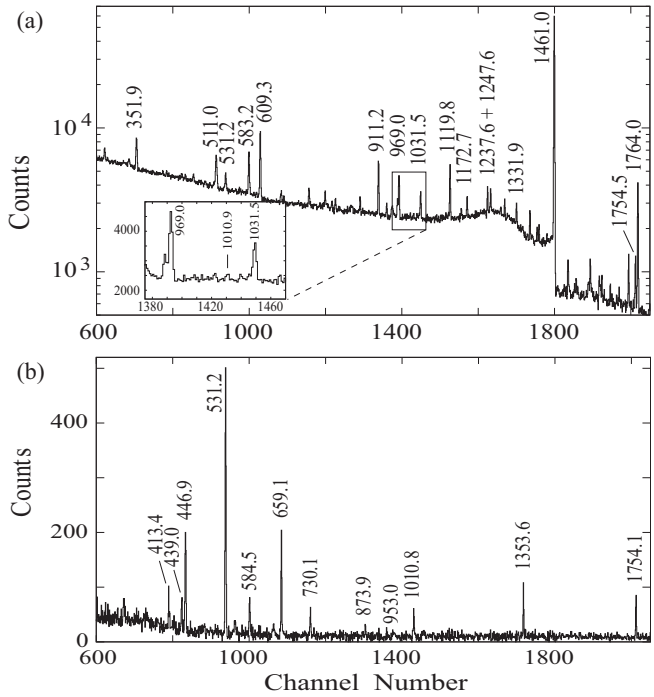

FIG. 7. (a) Total projection of the γ-S2 histogram on the S2 axis. (b) A spectrum gated on the γ axis on the 130.2-keV line, projected on the S2 axis. A nonlinear, constant-peak-width energy calibration was applied, the same as in Fig. 3. See the text for more details.

sees two pronounced discrete lines and no Compton-scattered events. However, the spectrum gated on the S2 axis on the 1754.5-keV peak, displayed in Fig. 8(c), shows both discrete lines and Compton-scattered events. The latter correspond to the backscattering of the strong 1754.5-keV γ line and contain in total more counts than the discrete lines.

Finally, in Fig. 8(d) we show a γ spectrum where the gate was set on the S2 axis on the 1545.9-keV region, corresponding to the excitation energy of the $9/2^+$ level in ^{89}Br. We do

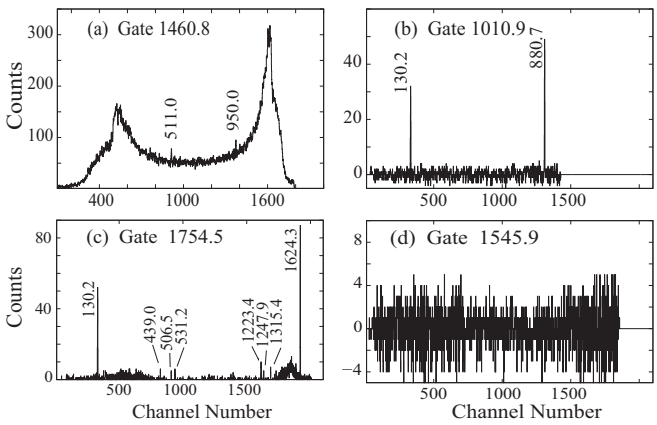

FIG. 8. γ-ray spectra gated on the S2 axis of the γ-S2 histogram: (a) gate on the 1460.8-keV line, (b) gate on the 1010.9-keV line, and (c) gate on the 1754.5-keV line. Spectrum (d) is gated on the region of the unobserved 1545.9-keV line. Energy calibration is as in Fig. 7.

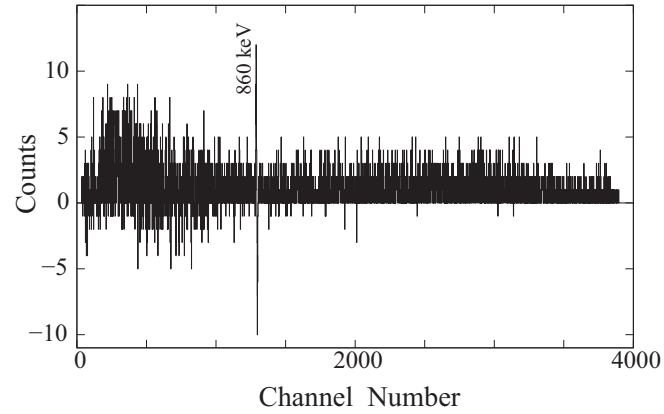

FIG. 9. Coincidence γ spectrum gated on the 1754.5-keV line of ^{89}Br. Lines are labeled with their γ energies in keV. A nonlinear, constant-peak-width energy calibration was applied, the same as in Fig. 3. The structure around 860 keV corresponds to cutting the "ridge" present in the $\gamma\gamma$ matrix due to backscaterring of the dominant, 2614.5-keV background line.

not see any trace of the 1039.2-506.7-keV, strongest decay cascade of this level, reported in Ref. [10].

In Fig. 9 we show a γ spectrum gated on the 1754.5-keV line, which suggest a strong direct population of the 1754.5-keV level in β decay. Indeed, in the spectrum, which spans the energy range from 0 to 6 MeV, one can not identify, in the present data, any discrete line feeding the 1754.5-keV level.

3. $\log_{10} ft$ values of levels in ^{89}Br

Using the I_γ values, shown in Table II, we calculated feeding of levels in ^{89}Br in β^- decay of ^{89}Se, also shown in the table. The β feedings were converted into corresponding $\log_{10} ft$ values, using the LOGFT program [26]. We assumed a 20(10)% feeding for the ground state of ^{89}Br, a value similar to that reported in ^{87}Br [8], and a 6(2)% β-n decay branch for the ground state of ^{89}Se, estimated in the present work (see Sec. III C 3).

The $\log_{10} ft$ values obtained are characteristic of the forbidden β^- transitions for most of the levels in ^{89}Br, except for the 1754.5-keV level, which is most likely populated by an allowed, Gamow-Teller transition.

One should stress that the $\log_{10} ft$ values (and their uncertainties) listed in Table II are lower limits, considering that there may be unobserved γ transitions feeding levels. As seen in Fig. 6 there are many weak high-energy transitions possibly populating the 130.2-keV level.

4. Spin-parity assignments to levels of ^{89}Br

The low statistics of the present measurement did not allow any analysis of angular correlations in γ-γ cascades of ^{89}Br. The proposed spins in ^{89}Br are based on the decay branching and $\log_{10} ft$ values observed in this work and on the information from prompt-γ fission [10].

Considering the available s.p. proton configurations in ^{89}Br one expects negative parity for most of the low-energy levels

in this nucleus. The forbidden character of β transitions to these levels and the allowed transition to the 1754.5-keV level indicate positive parity of the latter.

With the information from Ref. [10] we assign spin-parities $(5/2)^-$, $(3/2)^-$, $(7/2)^-$, $(5/2)^-$, and $(7/2)^-$ to the ground state and 130.2-, 506.5-, 531.2-, and 953.0-keV excited levels, respectively.

Tentative spin-parities $(3/2)^-$ and $(1/2)^-$ are proposed for the 439.0- and 446.9-keV levels respectively. The $5/2^-$ option is less likely because these levels were not seen in the prompt-γ work [10], which suggests their non-yrast character (as discussed in Ref. [27], fission process populates predominantly yrast levels).

For the 584.7-keV level, which decays to the $(3/2)^-$ level at 130.2 keV but not to the $(5/2^-)$ ground state, a tentative $(1/2)^-$ spin-parity is proposed, as the most likely option. This level was not reported in prompt-γ fission [10], which supports its low spin.

The 730.1-keV level has spin lower than 7/2, because it was not reported in prompt-γ fission [10] and its $\log_{10} ft = 6.29(7)$ suggests negative parity. Its spin should be higher than 1/2 because of the 199.0-keV decay to the $(5/2^-)$ level at 531.2 keV. Spin-parity $(3/2^-)$ is favored because of the 283.2-keV decay to the 446.9-keV level with the proposed spin-parity $(1/2^-)$.

The most likely spin-parity for the 1754.5-keV level is $(5/2)^+$, considering its $\log_{10} ft$ and γ decays to the $(7/2)^-$ levels at 953.0 keV and the $(3/2)^-$ level at 439 keV.

No assignment is made to other levels. We just note that their spins range from 1/2 to 7/2 and their parity is probably negative, considering their $\log_{10} ft$ values. Further suggestions are given in Sec. IV B.

C. Properties of the ground state of ^{89}Se

1. Half-life of the ^{89}Se ground state

To determine a more precise half-life of the ground state of ^{89}Se we fitted the time spectrum created by summing time spectra gated on the nine strongest γ lines populated in β^- decay of ^{89}Se, including the 130.2- and 1754.5-keV gates shown in Fig. 4. The new half-life of the ^{89}Se ground state obtained in this work is $T_{1/2} = 0.39(3)$ s.

2. Spin-parity of the ^{89}Se ground state

With the odd neutron occupying the $d_{5/2}$ shell one would expect the spin-parity of the ^{89}Se ground state to be $5/2^+$, as tentatively adopted in the compilation [24], based on systematics and shell-model predictions, although other calculations suggested spin-parity $3/2^+$ [28].

The $\log_{10} ft$ values listed in Table II are consistent with positive parity of the ^{89}Se ground state.

The β^- decay of the ^{89}Se ground state clearly populates $(7/2^-)$ levels at 506.5 and 953.0 keV in ^{89}Br. This indicates that the spin of the ^{89}Se ground state is higher than 1/2. On the other hand, the present analysis does not show any sign of the population of the $9/2^+$ at 1545.9 keV in ^{89}Br, observed in prompt-γ fission [10]. This indicates that the spin of the ground state of ^{89}Se should be lower than 7/2.

Of the two options left the $5/2^+$ spin-parity assignment to the ground state of ^{89}Se is less likely, because of the nonpopulation of the $9/2^+$ level. Although the $\log_{10} ft = 6.3$ value for $(7/2)^-$ levels might suggest spin-parity $5/2^+$, it is quite likely that these values will increase in future, higher-statistic measurements.

Another argument in favor of the $3/2^+$ assignment steams from the analysis of the $\beta^- n$ decay channel of ^{89}Se (see Sec. III C 3), which most strongly populates the (2^-) level at 159.1 keV in ^{88}Br. The 3^- level at 272.8 keV receives weaker population and 4^- levels in ^{88}Br are not populated.

Considering the above, we propose a tentative spin-parity $(3/2)^+$ assignment for the ground state of ^{89}Se.

A similar $3/2^+$ spin-parity was assigned in Ref. [8] to the ground state of the ^{87}Se isotope, confirming the earlier proposition of Ref. [29] where it was explained as due to the so-called $j-1$ anomalous coupling of the three neutrons in the $d_{5/2}$ shell. It is an interesting question to ask whether a similar effect is also present at the $N = 55$ isotonic line.

3. $\beta^- n$ decay of ^{89}Se

In the present work we could observe some γ decays in ^{88}Br populated via the $\beta^- n$ decay channel of ^{89}Se. The strongest γ line of ^{88}Br seen at 159.1-keV in our data corresponds to the decay of the (2^-) level reported at 159.1 keV in both, β^- decay of ^{88}Se [7] and in neutron-induced fission of ^{235}U [5]. In the spectrum gated on the 159.1-keV line in the $\gamma\gamma$ histogram, the 113.9-keV line, corresponding to the decay of the 3^- at 270.2 keV in ^{88}Br is clearly seen, but decays of 4^- levels, reported in Refs. [5,7] are not observed in the present work.

The γ intensity of the 159.1-keV line found in the singles spectrum is a 0.04(1) fraction of the summed γ intensity of transitions feeding the ground state of ^{89}Br in β^- decay of ^{89}Se. Because the mixing ratios of the 130.2- and 159.1-keV transitions as well as the direct population in β^- of the ground state of ^{89}Br are not known, we cannot properly determine the total intensity of the β^- decay of ^{89}Se but a rough estimate suggests that 3% of the β^- decay of ^{89}Se goes through the 159.1 keV line in ^{88}Br. However, there are more ground-state transitions in ^{88}Br, as reported in [5,7]. Of these, the 259.1- and 262.3-keV lines are seen in our data with their total singles intensity comparable to that of the 159.1-keV line. We do not observe other ground-state transitions in ^{88}Br reported in [7] but the population in β^- decay of ^{88}Se may differ from the population in $\beta^- n$ decay of ^{89}Se.

Based on the above data we roughly estimate the $\beta^- n$ decay branch of ^{89}Se to be 6(2)%, which is near the 7.8(25)% value reported in the compilation [24].

IV. DISCUSSION

In this section we will first discuss possible structure of excitations in ^{89}Br looking at the systematic behavior of analogous excitations in the neighboring, odd-Z nuclei and then compare them against the predictions of the large-scale shell model.

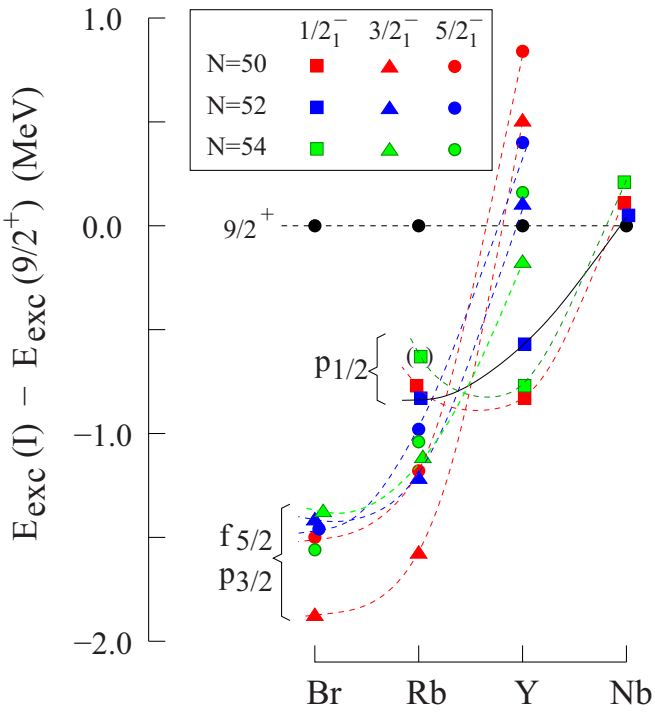

FIG. 10. Energies of $1/2^-_1$, $3/2^-_1$, and $5/2^-_1$ levels in the $N = 50$, $N = 52$, and $N = 54$ odd-Z isotones. Energies are drawn relative to $9/2^+$ excitations. The data are taken from Refs. [8–10,24,37–40] and the present work. Dashed lines are drawn to guide the eye.

A. Phenomenological description

One immediate observation when looking at the low-energy excitation scheme of ^{89}Br as well as that of ^{87}Br [8] is the rather large number of excited levels below 2 MeV (i.e., roughly, within the pairing-gap range). With only three protons close to the Fermi level, $\pi f_{5/2}$, $\pi p_{3/2}$, and $\pi p_{1/2}$, one would expect a lower number of excitations in a single-well, spherical potential. There are, of course, extra levels due to residual interactions between these states but one wonders whether they can account for all the observed states or should one rather consider the existence of more than one minimum in the potential. The latter option has already been considered in the region with a prolate [30,31] minimum present in addition to the spherical one. In such a case the emerging collectivity would split the $p_{3/2}$ and $f_{5/2}$ spherical proton shells into Nilsson-type orbits, increasing the number of distinct s.p. levels.

1. Low-spin, single-particle levels of negative parity

The low-energy, low-spin structures of ^{87}Br and ^{89}Br are quite similar. By analogy with the neighboring ^{87}Br [9] and ^{91}Rb [24] we propose that the ground state and the first excited state at 130.2 keV in ^{89}Br correspond to the odd proton occupying the close-lying $\pi p_{3/2}$ and $\pi f_{5/2}$ orbitals. Therefore one expects spin-parity of $3/2^-$ and $5/2^-$ for these two states in ^{89}Br, respectively, as proposed by Nyako *et al.* [10].

Figure 10 shows energies of the $1/2^-_1$, $3/2^-_1$, and $5/2^-_1$ levels relative to the excitation of the $9/2^+$ level in $N = 54$ isotones, including the present data for ^{89}Br. For comparison, also shown are the analogous energies in the $N = 50$ and $N = 52$ isotones.

The trends of the energies of the low-spin levels in Fig. 10 are remarkably similar in all three isotonic lines. This supports the spin-parity assignments to these levels and suggests their similar structure. One notes some deviation of the $1/2^-_1$ point at ^{91}Y and of $3/2^-_1$ level in ^{85}Br and ^{87}Rb.

The quickly varying energies of proton excitations with the proton number Z in Fig. 10 reflect the population of subsequent proton orbitals when the proton Fermi level is rising. This is similar to the quickly varying energies of neutron excitations with the neutron number, driven by the population of subsequent neutron orbitals in the isotopic chains (see, e.g., Figs. 1–3 in Ref. [32]). The populations of the $3/2^-_1$ and $5/2^-_1$ levels are very similar as a function of Z, confirming close proximity of the $f_{5/2}$ and $p_{3/2}$ shells observed previously [11,33–35]. The $p_{1/2}$ shell is populated at higher Z.

2. Positive-parity levels due to the $\pi g_{9/2}$ shell

A distinct difference between the scheme of excitations in ^{89}Br, populated in β^- decay of the ^{89}Se ground state and the scheme of ^{87}Br populated in β^- decay of the ^{87}Se ground state is the lack of the $9/2^+$ excitation in the former, as seen in Fig. 5. The difference is striking, because the same $(3/2^+)$ spin-parity was proposed for the ground states of both ^{87}Se and ^{89}Se mother nuclei, and the $9/2^+$ level of the same $\pi g_{9/2}$ origin is present in both nuclei at similar excitation energies of 1463.9 keV in ^{87}Br [8,9] and of 1545.9 keV in ^{89}Br [10].

The $9/2^+$ level in ^{87}Br is not populated directly in β^- decay of the $(3/2^+)$ g.s. of ^{87}Se. It receives its population via γ decays of high-energy, low-spin levels of positive parity, cascading to the $9/2^+$ level. A similar structure of these levels favors their strong links. Analogous cascades of levels with spins decreasing with the increasing energy, feeding the "opposite-parity," high-spin isomers were observed before in other nuclei and called "structurally controlled γ-ray cascades" [36].

In ^{89}Br one most likely observes a $5/2^+$ excitation of such nature at 1754.5 keV. Its $\pi g_{9/2}$ origin is indicated by the strong beta decay to this level, which most likely corresponds to the $\nu g_{7/2} \rightarrow \pi g_{9/2}$ Gamow-Teller transition. The expected $E2$ decay of the 1754.5 keV level, to the known $9/2^+$ level at 1545.9 keV of 208 keV, is not seen because it cannot compete with the 1754.5- and 1624.3-keV $E1$ decays. In ^{87}Br the analogous $E2$ decay has an energy of 420 keV, which allows about 30 times faster decay. The 420 keV branch in ^{87}Br corresponds to 0.025 of the total γ-decay intensity of the $(5/2^+)$ level at 1883.6 keV [8]. Thus, in ^{89}Br one might expect a 0.001 decay branch for the 208 transition, which is below the 0.003 limit of observation in the present work.

3. Collective versus single-particle excitations

The $7/2^-$ levels in ^{89}Br at 506.5 and 953.0 keV, strongly populated in cold-neutron fission [10], are only weakly populated in β decay. One reason, mentioned above, is that the spin-parity of the ground state of the ^{89}Se mother nucleus is $(3/2)^+$ rather than the previously assigned $(5/2^+)$ [24]. An-

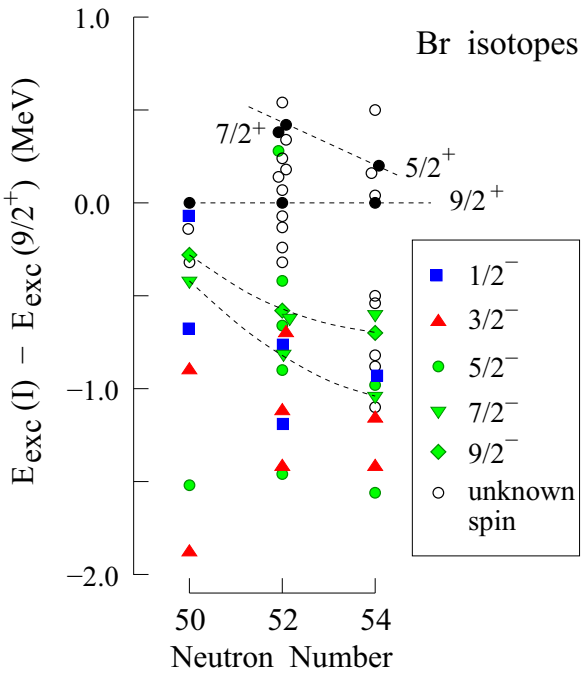

FIG. 11. Systematics of low-spin levels in the Br isotopes drawn relative to the $9/2^+$ excitations. The data are taken from Refs. [8–10,24,37–40] and the present work. Dashed lines are drawn to guide the eye.

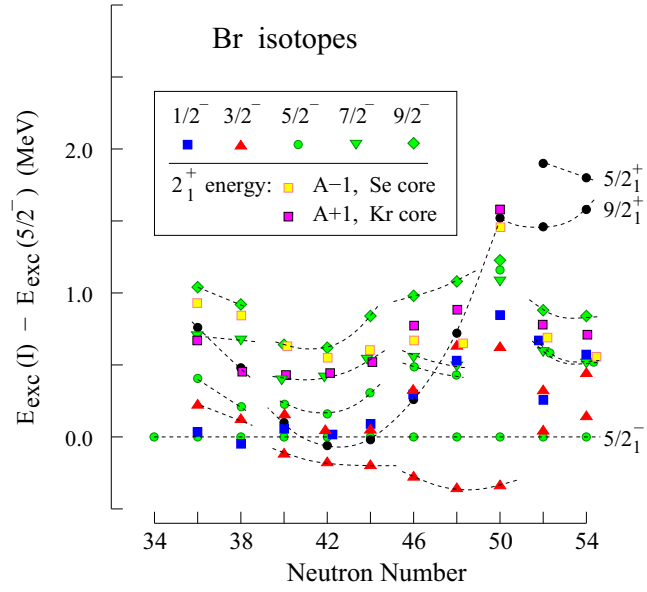

FIG. 12. Systematics of low-spin levels in bromine isotopes drawn relative to the $5/2^-_1$ excitations. The data are taken from Refs. [8–10,37,41–47] and the present work. Lines are drawn to guide the eye.

other reason may be a collective nature of these levels because there is no proton orbital with spin-parity $7/2^-$ available.

Figure 11 shows excitation energies in bromine isotopes up to 2 MeV above the ground state, which are drawn relative to the energy of the $9/2^+$ level. There is a significant increase in the number of levels at $N = 52$ and 54 compared to $N = 50$ (as seen in Fig. 6, many weak lines emerge, which could not be placed in the level scheme). These "extra" levels are, among others, probably due to neutron-pair excitations.

In Fig. 11 some excitations display regular trends, like the $7/2^-_1$ and $9/2^-_1$ levels, but generally it is not clear which levels with a given spin are related. To search for further regularities we show in Fig. 12 excitations of Br isotopes in a wider neutron range.

The choice of the $9/2^+$ level as a reference, which was optimal when showing systematic trends of proton levels along the proton number in Fig. 10, may be less useful when observing systematic trends of proton levels along the neutron number, because its position is influenced by proton-neutron residual interactions, which are particularly strong for intruder orbitals. Therefore, in Fig. 12 the $5/2^-_1$ level, expected to be a relatively unmixed $\pi f_{5/2}$ s.p. configuration, was taken as a reference.

In Fig. 12 the excitation energy of the $9/2^+_1$ level has, indeed, a pronounced minimum around $N \approx 42$, caused by the strong $\pi g_{9/2} - \nu g_{9/2}$ attraction. The collective strength is represented by the energy of the 2^+_1 excitation energy in the respective $A - 1$ Se and $A + 1$ Kr cores and is strongest around this neutron number.

The $5/2^+_1$ levels at $N = 52$ and $N = 54$ follow the trend of 2^+_1 excitations, suggesting that they are due to the $(\pi g_{9/2} \otimes 2^+_1)_j$ coupling.

Analogously, the $7/2^-_1$ and $9/2^-_1$ excitations probably correspond to the $3/2^-_1 \otimes 2^+_1$ and $5/2^-_1 \otimes 2^+_1$ couplings, respectively. Here the $3/2^-_1$ and $5/2^-_1$ levels are probably due to $\pi p_{3/2}$ and $\pi f_{5/2}$ origin, respectively.

There are also low-lying $1/2^-_1$, $3/2^-_2$ and $5/2^-_2$ levels, which follow the trend set by the collectivity, which suggest that they correspond to various couplings of this collectivity to single-particle excitations:

(i) The so-called anomalous coupling was reported in $N = 53$, even-Z isotones [29], where in addition to the low-energy $5/2^+_1$ level due to the odd neutron in the $d_{5/2}$ shell one observes a low-energy, $3/2^+_1$ level, which is produced by three neutrons in the $d_{5/2}$ shell, coupled with a collective excitation of the core. In Fig. 12, one sees $3/2^-_2$ levels close to the $5/2^-_1$ level, which may correspond to the $(\pi f^3_{5/2})_{j-1}$ anomalous coupling. The low-lying $3/2^-_2$ levels in ^{87}Br and ^{89}Br may be of the same origin.

(ii) The $1/2^-_1$ levels, which follow closely the $3/2^-_2$ levels, may correspond to the $j - 2$ anomalous coupling, proposed first in this region in ^{90}Rb [14] and observed before in the $N = 85$ isotones (see Fig. 3 in Ref. [48]). We note that the $1/2^-_1$ levels are not due to the $\pi p_{1/2}$ s.p. excitation expected at higher energies, as seen in Fig. 10.

(iii) The $5/2^-_2$ levels, which also have quite low excitation energies and follow the trend of $7/2^-_1$ levels, may correspond to another $(\pi f_{5/2} \otimes 2^+_1)_{j-1}$ not-fully-aligned coupling.

In the above discussion we proposed plausible explanations to many of the low-energy levels in odd-A bromine isotopes. However, there are still open questions, for example about the low-energy $1/2^-_2$ level in ^{87}Br. It is thus of interest to use model calculations to verify the above propositions.

B. Shell-model interpretation

The shell-model calculations were performed in a large valence space outside the ^{78}Ni core, including the $1f_{5/2}$, $2p_{3/2}$, $2p_{1/2}$, and $1g_{9/2}$ orbitals for protons and the $2d_{5/2}$, $3s_{1/2}$, $1g_{7/2}$, $1d_{3/2}$, and $1h_{11/2}$ orbitals for neutrons. The model and the parameters of the calculations are the same as used in Refs. [9,10] to describe ^{87}Br and ^{89}Br nuclei and as in studies of other nuclei in this region reported in Refs. [5–8,14]. The full-space diagonalization of the Hamiltonian was achieved using the shell-model code ANTOINE [49,50].

The calculated level scheme of ^{89}Br is compared to experimental data in Fig. 13. All the experimental, low-spin states have their theoretical counterparts, including four $3/2^-$ states. This supports spin-parity assignments proposed in this work.

The calculated states all have largely fragmented wave functions, without dominating components. As noted in Ref. [10] the proximity of the $p_{3/2}$ and $f_{5/2}$ orbitals favors a large mixing and the development of deformation in this region. The $p_{1/2}$ orbital is also populated (from 0.4 to 0.9 particle) in all the low-spin states calculated, reaching the maximum of one particle in the first excited $1/2^-$ state. The $5/2^-$, $3/2^-$, and $1/2^-$ states share a common feature: the contribution of the $(\pi J^- \otimes \nu 0^+)$ configuration does not exceed 50% and decreases with excitation energy in favor of the $(\pi 3/2^-, 5/2^-, 1/2^- \otimes \nu 2^+)$ components of equal importance.

In addition to the ^{89}Br analysis, we compared experimental and theoretical systematic trends of low-energy excitations in the $N = 50$, $N = 52$, and $N = 54$ isotones. As seen in Fig. 14, general experimental and calculated trends agree well.

At $N = 50$, the purely proton wave functions have a simple structure. In ^{83}As 70% of the $5/2^-$ state corresponds to the $f^{-1}_{5/2}$ configuration and 77% of the $3/2^-$ state corresponds to the $p^1_{3/2}$ configuration. The lowest $1/2^-$ state is a mixture of different configurations where particles occupy these two orbitals with only 0.35 particle in $p_{1/2}$. With more protons, in ^{85}Br, ^{87}Rb, and ^{89}Y, one still finds the one-hole and one-particle configurations dominating the $5/2^-$ and $3/2^-$ states but the occupation of the $p_{1/2}$ orbital in the $1/2^-$ state grows to 0.84, 0.99, and 0.98 particle, respectively. After filling the $g_{9/2}$ orbital in ^{91}Nb the structure of the $3/2^-$ and $5/2^-$ states changes to become a $p^{-1}_{1/2}$ hole coupled to the $g^2_{9/2}$ configuration. This can be seen in Fig. 14 as the change in the trend of $3/2^-_1$ and $5/2^-_1$ levels between Y and Nb.

As discussed in the shell-model context in Ref. [51], the $N = 52$ and $N = 54$ isotones in this region exhibit quadrupole collectivity and even triaxiality. The increase of collectivity is easily noted in the computed wave functions. With an addition of only two neutrons the wave functions alter from over 70% in ^{83}As to ≈40% ^{85}As of pure one-particle one-hole contributions in the $3/2^-$ and $5/2^-$ states. These numbers decrease further in ^{87}As to about 30%, only.

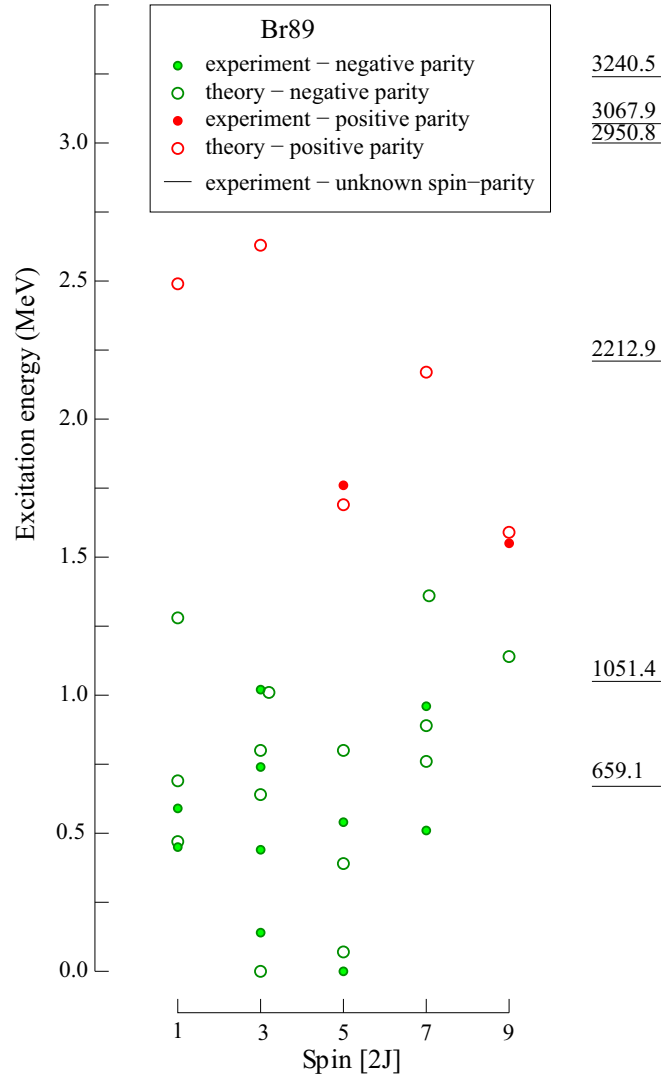

FIG. 13. Comparison of the experimental level scheme of the ^{89}Br nucleus with the results of large-scale shell-model calculations. See text for more comments.

Despite the increasing mixing in the wave functions when adding neutrons and protons, the theoretical excitation patterns in all three isotonic chains seen in Fig. 14 show a similar breakdown of the "parabolic" trend below Br isotopes. A large increase of the energy splitting between the $9/2^+$ level and the negative-parity states is observed in As isotopes as compared to Br isotopes.

The $9/2^+$ level in ^{83}As was proposed in Ref. [11] at 2779 keV. The recent work [52] questions this assignment, though without proposing any specific level instead, stating only that it might be one of their newly observed levels around 3 MeV. The present shell-model calculations predict this level at 2.53 MeV.

It is important to note that in Ref. [52] shell-model calculations within the same model space and using an effective interaction based on [53] were performed, predicting the position of the $9/2^+$ at 2.37 MeV, in good agreement with the current study. Earlier calculations of Ref. [54] using the

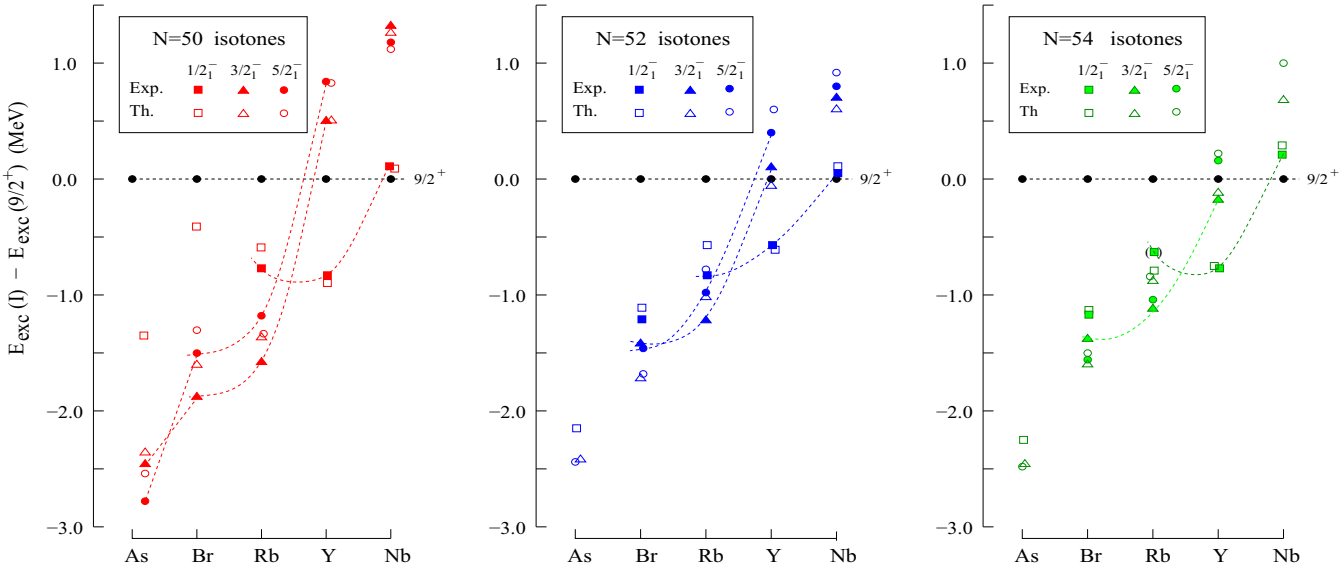

FIG. 14. Comparison of the experimental excitation energies of $N = 50$, $N = 52$, and $N = 54$ As-to-Nb isotones with the results of large-scale model calculations. The energies are drawn relative to the $9/2^+$ excitations. See text for more comments.

JJ4B-based effective interaction and a smaller model space also predicted a 2.5 MeV excitation energy for the $9/2^+$ state in ^{83}As. However, the $f_{5/2} - g_{9/2}$ splitting in the core differs a lot between those three interactions: it drops from 5.71 MeV in the present work to 3.95 MeV in Ref. [52] and to 3.39 MeV in Ref. [54]. Clearly, a better knowledge of positive-parity excitations in As and in Ga isotopes is required to refine the position of the proton orbitals in the ^{78}Ni core and the two-body matrix elements governing their evolution with proton and neutron numbers.

V. SUMMARY

Low-spin, excited states of the neutron-rich ^{89}Br nucleus populated in β^- decay of ^{89}Se have been studied for the first time, using a high-efficiency array of high-resolution Ge detectors after the JYFLTRAP Penning trap at the IGISOL facility. The level scheme of ^{89}Se was extended by twelve new levels and 31 new γ transitions. A spin-parity of $(3/2^+)$ has been proposed for the ground state of the ^{89}Se mother nucleus, replacing the $(5/2^+)$ assignment reported in databases. The Gamow-Teller β^- transition to the new 1754.5-keV level with spin $(5/2)^+$ indicates its $\pi g_{9/2}$-based configuration. Excitations based on $\pi p_{3/2}$ and $\pi f_{5/2}$ single-particle levels as well as their anomalous coupling were proposed to explain the low-energy excitation scheme of ^{89}Br. Systematic comparison with $N = 50$, $N = 52$, and $N = 54$ isotones was done to help the interpretation of levels in ^{89}Br. Low-spin excitations of ^{89}Br were compared to the large scale shell-model calculations to obtain further insight into their structure. The calculations reproduced well most of experimental excitation energies in ^{89}Br as well as in As–Nb nuclei along the three isotonic lines, supporting the proposed interpretations. In particular, the position of the $\pi g_{9/2}$ orbital and the associated $9/2^+$ excitations were discussed, providing some support for the excitation energy of the $9/2^+$ level in ^{83}As at around 2.8 MeV, proposed in our earlier work, though further studies are needed in this subject.

ACKNOWLEDGMENTS

This work has been supported by the National Science Centre under Contract No. DEC-2018/29/N/ST2/00707 and by the Academy of Finland under the Finnish Centre of Excellence Program 2012–2017 (Nuclear and Accelerator Based Physics Research at JYFL) and under Grants No. 275389, No. 284516, No. 312544, and No. 295207. This project has received funding from the European Union's Horizon 2020 European Nuclear Science and Application Research 2 under Grant Agreement No. 654002 (ENSAR2).

[1] K. Heyde and J. L. Wood, Rev. Mod. Phys. **83**, 1467 (2011).
[2] W. Urban, K. Sieja, T. Rząca-Urban, J. Wiśniewski, A. Blanc, M. Jentschel, P. Mutti, U. Köster, T. Soldner, G. de France, G. S. Simpson, C. A. Ur, A. G. Smith, and J. P. Greene, Phys. Rev. C **104**, 064309 (2021).
[3] K. Sieja, Universe **8**, 23 (2022).
[4] A. E. Stuchbery and J. L. Wood, Physics **4**, 697 (2022).
[5] M. Czerwiński, T. Rząca-Urban, W. Urban, P. Bączyk, K. Sieja, B. M. Nyako, J. Timar, I. Kuti, T. G. Tornyi, L. Atanasova, A. Blanc, M. Jentschel, P. Mutti, U. Köster, T. Soldner, G. de France, G. S. Simpson, and C. A. Ur, Phys. Rev. C **92**, 014328 (2015).
[6] W. Urban, K. Sieja, T. Materna, M. Czerwiński, T. Rząca-Urban, A. Blanc, M. Jentschel, P. Mutti, U. Köster, T. Soldner,

G. de France, G. S. Simpson, C. A. Ur, Ch. Bernards, C. Fransen, J. Jolie, J.-M. Regis, T. Thomas, and N. Warr, Phys. Rev. C **94**, 044328 (2016).
[7] M. Czerwiński, K. Sieja, T. Rząca-Urban, W. Urban, A. Płochocki, J. Kurpeta, J. Wiśniewski, H. Penttilä, A. Jokinen, S. Rinta-Antila, L. Canete, T. Eronen, J. Hakala, A. Kankainen, V. S. Kolhinen, J. Koponen, I. D. Moore, I. Pohjalainen, J. Reinikainen, V. Simutkin, A. Voss, I. Murray, and C. Nobs, Phys. Rev. C **95**, 024321 (2017).
[8] J. Wiśniewski, W. Urban, M. Czerwiński, J. Kurpeta, A. Płochocki, M. Pomorski, T. Rząca-Urban, K. Sieja, L. Canete, T. Eronen, S. Geldhof, A. Jokinen, A. Kankainen, I. D. Moore, D. A. Nestarenko, H. Penttilä, I. Pohjalainen, S. Rinta-Antila, A. de Roubin, and M. Vilén, Phys. Rev. C **100**, 054331 (2019).
[9] B. M. Nyako, J. Timár, M. Csatlós, Z. Dombrádi, A. Krasznahorkay, I. Kuti, D. Sohler, T. G. Tornyi, M. Czerwiński, T. Rząca-Urban, W. Urban, P. Baczyk, L. Atanasova, D. L. Balabanski, K. Sieja, A. Blanc, M. Jentschel, U. Köster, P. Mutti, T. Soldner *et al.*, Phys. Rev. C **103**, 034304 (2021).
[10] B. M. Nyako, J. Timár, M. Csatlós, Z. Dombrádi, A. Krasznahorkay, I. Kuti, D. Sohler, T. G. Tornyi, M. Czerwiński, T. Rząca-Urban, W. Urban, P. Bączyk, L. Atanasova, D. L. Balabanski, K. Sieja, A. Blanc, G. de France, M. Jentschel, U. Köster, P. Mutti *et al.* Phys. Rev. C **104**, 054305 (2021).
[11] P. Bączyk, W. Urban, D. Złotowska, M. Czerwiński, T. Rząca-Urban, A. Blanc, M. Jentschel, P. Mutti, U. Köster, T. Soldner, G. de France, G. S. Simpson, and C. A. Ur, Phys. Rev. C **91**, 047302 (2015).
[12] G. S. Simpson, W. Urban, K. Sieja, J. A. Dare, J. Jolie, A. Linneman, R. Orlandi, A. Scherillo, A. G. Smith, T. Soldner, I. Tsekhanovich, B. J. Varley, A. Złomaniec, J. L. Durell, J. F. Smith, T. Rząca-Urban, H. Faust, I. Ahmad, and J. P. Greene, Phys. Rev. C **82**, 024302 (2010).
[13] W. Urban, K. Sieja, G. S. Simpson, T. Soldner, T. Rząca-Urban, A. Złomaniec, I. Tsekhanovich, J. A. Dare, A. G. Smith, J. L. Durell, J. F. Smith, R. Orlandi, A. Scherillo, I. Ahmad, J. P. Greene, J. Jolie, and A. Linneman, Phys. Rev. C **85**, 014329 (2012).
[14] M. Czerwiński, T. Rząca-Urban, W. Urban, P. Bączyk, K. Sieja, J. Timar, B. M. Nyako, I. Kuti, T. G. Tornyi, L. Atanasova, A. Blanc, M. Jentschel, P. Mutti, U. Köster, T. Soldner, G. de France, G. S. Simpson, and C. A. Ur, Phys. Rev. C **93**, 034318 (2016).
[15] J. Litzinger, A. Blazhev, A. Dewald, F. Didierjean, G. Duchêne, C. Fransen, R. Lozeva, K. Sieja, D. Verney, G. de Angelis *et al.*, Phys. Rev. C **92**, 064322 (2015).
[16] I. D. Moore, T. Eronen, D. Gorelov, J. Hakala, A. Jokinen, A. Kankainen, V. Kolhinen, J. Koponen, H. Penttilä, I. Pohjalainenet, M. Reponen, J. Rissanen, A. Saastamoinen, S. Rinta-Antila, V. Sonnenschein, and J. Äystö, Nucl. Instrum. Methods Phys. Res., Sect. B **317**, 208 (2013).
[17] P. Karvonen, I. D. Moore, T. Sonoda, T. Kessler, H. Penttilä, K. Peräjärvi, P. Ronkanen, and J. Äystö, Nucl. Instrum. Methods Phys. Res., Sect. B **266**, 4794 (2008).
[18] A. Nieminen, J. Huikari, A. Jokinen, and J. Äystó, Nucl. Instrum. Methods Phys. Res., Sect. A **469**, 244 (2001).
[19] T. Eronen, V. S. Kolhinen, V.-V. Elomaa, D. Gorelov, U. Hager, J. Hakala, A. Jokinen, A. Kankainen, P. Karvonen, S. Kopecky, I. D. Moore, H. Penttilä, S. Rahaman, S. Rinta-Atila, J. Rissanen, A. Saastamoinen, J. Szerypo, C. Weber, and J. Äystö, Eur. Phys. J. A **48**, 46 (2012).
[20] G. Savard, S. Becker, G. Bollen, H.-J. Kluge, R. B. Moore, T. Otto, L. Schweikhard, H. Stolzenberg, and U. Wiess, Phys. Lett. A **158**, 247 (1991).
[21] G. R. Gilmore, *Practical Gamma-Ray Spectrometry*, 2nd ed. (Wiley, New York, 2008).
[22] K. Rengan, J. Lin, M. Zendel, and R. A. Meyer, Nuclear Instruments and Methods in Physics Research **197**, 427 (1982).
[23] T. Rzaca-Urban, K. Sieja, W. Urban, M. Czerwiński, A. Blanc, M. Jentschel, P. Mutti, U. Köster, T. Soldner, G. de France, G. S. Simpson, and C. A. Ur, Phys. Rev. C **95**, 064302 (2017).
[24] B. Singh, Nucl. Data Sheets **114**, 1 (2013).
[25] T. Rząca-Urban, W. Urban, M. Czerwiński, J. Wiśniewski, A. Blanc, H. Faust, M. Jentschel, P. Mutti, U. Köster, T. Soldner, G. de France, G. S. Simpson, and C. A. Ur, Phys. Rev. C **98**, 064315 (2018).
[26] Tools and Publications, http://www.nndc.bnl.gov
[27] I. Ahmad and W. R. Phillips, Rep. Prog. Phys. **58**, 1415 (1995).
[28] P. Möller, J. R. Nix. and K.-L. Kratz, At. Data Nucl. Data Tables **66**, 131 (1997).
[29] T. Rząca-Urban, M. Czerwiński, W. Urban, A. G. Smith, I. Ahmad, F. Nowacki, and K. Sieja, Phys. Rev. C **88**, 034302 (2013).
[30] M. G. Porquet, T. Venkova, A. Astier, I. Deloncle, A. Prévost, F. Azaiez, A. Buta, D. Curien, O. Dorvaux, G. Duchêne, B. J. P. Gall, F. Khalfallah, I. Piqueras, M. Rousseau, M. Meyer, N. Redon, O. Stêzowski, R. Lucas, and A. Bogachev, Eur. Phys. J. A **28**, 153 (2006).
[31] I. N. Gratchev, G. S. Simpson, G. Thiamova, M. Ramdhane, K. Sieja, A. Blanc, M. Jentschel, U. Köster, P. Mutti, T. Soldner, G. de France, C. A. Ur, and W. Urban, Phys. Rev. C **95**, 051302(R) (2017).
[32] W. Urban, T. Rząca-Urban, J. Wiśniewski, J. Kurpeta, A. Płochocki, J. P. Greene, A. G. Smith, and G. S. Simpson, Phys. Rev. C **102**, 024318 (2020).
[33] L. Käubler, K. D. Schilling, R. Schwengner, F. Dönau, E. Grosse, D. Belic, P. von Brentano, M. Bubner, C. Fransen, M. Grinberg, U. Kneissl, C. Kohstall, A. Linnemann, P. Matschinsky, A. Nord, N. Pietralla, H. H. Pitz, M. Scheck, F. Stedile, and V. Werner, Phys. Rev. C **65**, 054315 (2002).
[34] D. Verney, F. Ibrahim, C. Bourgeois, S. Essabaa, S. Galès, L. Gaudefroy, D. Guillemaud-Mueller, F. Hammache, C. Lau, F. Le Blanc, A. C. Mueller, O. Perru, F. Pougheon, B. Roussière, J. Sauvage, and O. Sorlin (PARRNe Collaboration), Phys. Rev. C **76**, 054312 (2007).
[35] A. Gade, T. Baugher, D. Bazin, B. A. Brown, C. M. Campbell, T. Glasmacher, G. F. Grinyer, M. Honma, S. McDaniel, R. Meharchand, T. Otsuka, A. Ratkiewicz, J. A. Tostevin, K. A. Walsh, and D. Weisshaar, Phys. Rev. C **81**, 064326 (2010).
[36] W. B. Walters, E. A. Henry, and R. A. Meyer, Phys. Rev. C **29**, 991 (1984).
[37] B. Singh, ^{85}Br Adopted Levels, Gammas, ENSDF-Evaluated, 2015, http://www.nndc.bnl.gov
[38] T. D. Johnson and W. D. Kulp, Nucl. Data Sheets **129**, 1 (2015).
[39] C. M. Baglin, Nucl. Data Sheets **112**, 1163 (2011).
[40] C. M. Baglin, Nucl. Data Sheets **114**, 1293 (2013).
[41] K. Abusaleem and B. Singh, Nucl. Data Sheets **112**, 133 (2011).
[42] B. Singh and J. ChenNucl. Data Sheets **158**, 1 (2019).

[43] A. Negret and B. Singh, Nucl. Data Sheets **114**, 841 (2013).
[44] B. Singh, ^{77}Br Adopted Levels, Gammas, ENSDF-Evaluated, 2020, http://www.nndc.bnl.gov
[45] B. Singh, Nucl. Data Sheets **135**, 193 (2016).
[46] C. M. Baglin, Nucl. Data Sheets **109**, 2257 (2008).
[47] E.A. McCutchan, Nucl. Data Sheets **125**, 201 (2015).
[48] W. Urban, W. R. Phillips, I. Ahmad, J. Rękawek, A. Korgul, T. Rząca-Urban, J. L. Durell, M. J. Leddy, A. G. Smith, B. J. Varley, N. Schulz, and L. R. Morss, Phys. Rev. C **66**, 044302 (2002).
[49] E. Caurier and F. Nowacki, Acta Phys. Pol. B **30**, 705 (1999).
[50] E. Caurier, G. Martinez-Pinedo, F. Nowack, A. Poves, and A. P. Zuker, Rev. Mod. Phys. **77**, 427 (2005).
[51] K. Sieja, T. R. Rodriguez, K. Kolos, and D. Verney, Phys. Rev. C **88**, 034327 (2013).
[52] K. Rezynkina, D. D. Dao, G. Duchêne, J. Dudouet, F. Nowacki, E. Clément, A. Lemasson, C. Andreoiu, A. Astier, G. de Angelis, G. de France *et al.*, Phys. Rev. C **106**, 014320 (2022).
[53] K. Sieja, F. Nowacki, K. Langanke, and G. Martínez-Pinedo, Phys. Rev. C **79**, 064310 (2009).
[54] E. Sahin, G. de Angelis, G. Duchene, T. Faul, A. Gadea, A. F. Lisetskiy, D. Ackermann, A. Algora, S. Aydin, F. Azaiez, D. Bazzacco *et al.*, Nucl. Phys. A **893**, 1 (2012).